LA-UR- 09-0K487

Approved for public release;
distribution is unlimited.

Title:	Radio-Frequency Measurements of UNiX Compounds (X = Al, Ga, Ge) in High Magnetic Fields
Author(s):	A. M. Alsmadi, S. Alycones, Charles H. Mielke, D. R. McDonald, Vivien Zapf, Moaz M. Altarawneh, Alex H. Lacerda, S. Chang, Sourav Adak, Kothapalli Karunakar, and Heinz Nakotte
Intended for:	Journal

Los Alamos
NATIONAL LABORATORY
EST. 1943

Form 836 (7/06)

Radio-Frequency Measurements of UNiX Compounds (X = Al, Ga, Ge) in High Magnetic Fields

A. M. Alsmadi and S. Alyones
Physics Department, The Hashemite University, 13115 Zarqa, Jordan

C. H. Mielke, R. D. McDonald, V. Zapf, M. M. Altarawneh, and A. Lacerda
National High Magnetic Field Laboratory, Pulsed Field Facility, Los Alamos National Laboratory, Los Alamos, NM 87545

S. Chang
NIST Center for Neutron Research, National Institute of Standards and Technology, Gaithersburg, MD 20899

S. Adak, K. Kothapalli and H. Nakotte
Physics Department, New Mexico State University, Las Cruces, NM 88003

Abstract

We performed Radio-Frequency (RF) skin-depth measurements of antiferromagnetic UNiX compounds (X = Al, Ga, Ge) in an applied magnetic fields up to 60 T in the temperature range from 1.4 up to about 60 K. Magnetic fields are applied along different crystallographic directions and RF penetration-depth measurements were done using a tunnel diode oscillator (TDO). The TDO couples the sample to the inductive element of a resonant tank circuit, and the shift in the resonant frequency Δf of the circuit is measured. The UNiX compounds exhibit (sometimes multiple) field-induced magnetic transitions in applied magnetic fields at low temperatures, and those transitions are accompanied by a drastic change in Δf. The results of our skin-depth measurements were compared with previously published B-T phase diagrams for these three compounds.

Introduction

Uranium compounds have been the subject of intense studies in the past decades because of the specific nature of U 5*f*-electron magnetism. The *5f* electrons of U are found to be intermediate between the delocalized *d* electrons of the transition metals and the well-localized 4*f* electrons of the lanthanides. For uranium compounds, there are two

mechanisms, which lead to the delocalization the 5*f* electrons; the direct 5*f*-5*f* overlap and the 5*f*-ligand hybridization [1]. However, while 5*f*-ligand hybridization can cause delocalization of the 5*f* states (suppression of 5*f* moments), it can also mediates indirect exchange interaction between them and thus promote long-range magnetic order. Another striking feature for uranium compounds is the huge magnetocrystalline anisotropy, and hybridization effects are again believed to play a key role in its origin.

Ternary UTX intermetallic compounds (T = transition metal and X = *p*-electron element) provide a rich system for the study of the role of the 5*f*-ligand hybridization and the formation of the uranium magnetic moments [1,2]. UTX compounds were found to crystallize mainly in four different crystal structures: the cubic MgAgAs, the hexagonal Fe_2P, the hexagonal $CaIn_2$ and the orthorhombic $CeCu_2$ types of structures or its ordered variants [2]. The formation of a specific structure seems to be connected with the number of *d* electrons in the transition metal [3]. The two largest groups of isostructural compounds are those with the hexagonal Fe_2P (ordered variant: ZrNiAl) type and the orthorhombic $CeCu_2$ (ordered variant: TiNiSi) type of structure. For X = Si or Ge the $CeCu_2$ (or TiNiSi) structure is obtained, whereas most of the compounds with larger X atoms, such as Al and Ga, typically crystallize in the ZrNiAl-type structure [4].

Systematic study of UTX compounds provided some general trends for the development of magnetism of UTX compounds, in particular, the size of magnetic 5*f* moment and the magnetic ordering temperatures [3]. However, there is still limited understanding about the main mechanisms that are responsible for the formation of the (often complex) magnetic structures and (often multiple) magnetic transitions between different phases.

Magnetic structures arise from a complex balance of interactions that are influenced by thermodynamic parameters like temperature, external pressure and magnetic fields. The study of field-induced magnetic transitions can therefore provide some insight into the strength of exchange interactions in antiferromagnetic UTX compounds. It is common to refer to these transitions as metamagnetic transitions, in analogy to the metastable (metamagnetic) state that is induced above a critical field, B_C. Metamagnetic transitions take place in a magnetic field sufficient to overcome the antiferromagnetic interactions and to modify the magnetic structure. This modification of the magnetic structure is often connected with a change of the translational symmetry, and is usually accompanied by a noticeable change in the magnetoresistance [1]. As mentioned above, the magnetic anisotropy in uranium compounds is huge, and metamagnetic transitions in these compounds often occur in the 10-60 T range [1]. Therefore, the study of metamagnetic transitions in uranium compounds typically requires the use of pulsed magnetic fields. Although magnetoresistance measurements are done commonly in pulsed fields, there are technological challenges for magnetoresistance studies, e.g. pick-up of induced electronic noise in leads, integrity of resistance contacts and their contact resistance, eddy-current effects, magnetic torque (rotation) effects in the sample during the field pulse.

Here, we present the measurements of the Radio-Frequency (RF) skin-depth for antiferromagnetic UNiX (T = Ni, and X = Al, Ga, Ge) in magnetic field up to 60 T, applied along different crystallographic directions at a wide range of temperatures. In table 1, we summarize the crystal structure, the ordering temperatures ,T_N, and transition fields, B_C for antiferromagnetic UNiX compounds presented in this study.

An alternative to magnetoresitance is Radio-Frequency (RF) skin-depth technique is a very useful probe of magnetotransport since the skin depth of the sample can be related to its complex conductivity, which can be converted to its resistivity [6-8]. Unlike magnetoresistance, RF skin-depth is a noncontact technique, making use of a tunnel diode oscillator (TDO), and there are fewer experimental challenges connected with doing those. However, the RF technique is a relatively new technique, and it has been used mostly for measurements on semi-conductors and insulators, such as high-T_C superconductors [7]. Recently, however, it was successfully used in metallic samples [8] and on doped insulators that showed metallic behavior [9].

Encouraged by such reports, we started to investigate the possibility of using RF skin depth measurements in uranium compounds. Our preliminary results for UNiAl, UNiGa and UNiGe [10] showed that RF skin-depth measurements can be used for the essentially metallic UTX compounds [10]. In particular, we found a direct correspondence between the features in RF measurements and magnetoresistance [10]. However, our previous studies were done only at liquid-helium temperature with the magnetic field applied only along the easy axis direction(s).

Here, we present extended studies of RF skin-depth at a various temperatures for the three UNiX compounds. Taking all the anomalies in the RF skin-depth measurements, we compare the results with the previously published B-T phase diagrams for these compounds.

Experimental

The experiments were performed on high purity single crystals using the 60 T short-pulse magnet at the Pulsed Field Facility, NHMFL, Los Alamos National Laboratory. The experiments were performed on the same crystals used in the previous study [10]. Bar-shaped sample (typically 0.5 × 0.5 × 4mm) were cut parallel and perpendicular to the easy magnetization directions.

The Radio-Freqency (RF) skin-depth measurements were done using a tunnel-diode oscillator (TDO) with a resonance frequency of $f = 1/2\pi\sqrt{LC}$. The TDO is an RF tank-circuit oscillator, for which the losses in the LC circuit are compensated by biasing the tunnel diode in the negative resistance region of its I-V characteristic [11]. Cryogenic temperatures are necessary to provide a large enough negative resistance to cause the tank circuit to oscillate. In the TDO method, the RF skin depth is measured by coupling the sample to the coil of the tank circuit and measuring the shift in the resonant frequency. When a magnetic sample is inserted into a tank coil, the inductance L is shifted by a small amount ΔL, which is proportional to the alternating current (a.c.)

susceptibility χ. As a result, the resonance frequency is shifted by Δf according to the relation $\frac{\Delta f}{f} = -\frac{\Delta L}{2L}$. The shift in the resonance frequency Δf is related to the resistivity ρ for metallic samples through the skin depth $\delta = \sqrt{\rho/\pi\mu_0 f}$, where μ_0 is the permittivity of free space. The change of resonance frequency is related to the shift in the skin depth as $\frac{\Delta f}{f} = -\frac{G\Delta\delta}{\delta}$, where G is the geometrical factor that depends on the sample and the coil geometries [8].

The RF skin depth measurements are commonly referred to as complex-conductivity in the literature. The frequency (and amplitude) shifts reflect the change in both the real and imaginary components of the conductivity. So this technique is sensitive to the dielectric (permittivity: ε_r) and the magnetic (permeability: μ_r) material properties. This technique has a high sensitivity of the order of 1 part in 10^9, and the experimental setup is relatively simple, and the non-contact method avoids damage to the sample. A more detailed description of the experimental set up used in the studies presented here is discussed in reference 7.

Results and Discussions

I. UNiAl

UNiAl crystallizes in the hexagonal ZrNiAl-type structure [1]. UNiAl is best described as an itinerant 5*f*-electron antiferromagnet (AF) with $T_N = 19.3\,\mathrm{K}$ [1]. Single-crystal studies reveal that UNiAl exhibits a large magnetic anisotropy with the easy magnetization direction along the hexagonal *c*-axis [12-15] and it can be classified as a moderate heavy-fermion system since an electronic contribution to the low-temperature specific heat of $\gamma = 164\ mJ/molK^2$ was reported [16-18]. At low temperatures, this compound undergoes a metamagnetic transition for the magnetic field along *c*-axis, and the critical field was found to be equal to $B_C = 11.35\,\mathrm{T}$ at 1.7 K [14].

Figure 1 displays the anisotropic behavior of the measured relative frequency shift of the tank circuit $\Delta f/f_{B=0}$ for UNiAl as a function of applied magnetic fields at 1.5 K. When the field is applied along the *c* axis, we observe a sudden reduction in $\Delta f/f_{B=0}$ at $B_C = 11.1$ T. For fields applied perpendicular to the *c* axis, there is no similar transition, but just a smooth and continuous decrease in $\Delta f/f_{B=0}$. This anisotropic behavior in $\Delta f/f_{B=0}$ is consistent with the magnetic anisotropy reported from previous bulk studies on single-crystalline UNiAl [14].

Figure 2 shows the field dependence of the measured relative frequency shift $\Delta f/f_{B=0}$ in UNiAl at different temperatures for fields applied along the *c* axis. The

frequency shift for up- and down-sweeps of the field is shown only for T = 1.5 K, while for other temperatures only the results from up- sweeps are shown. The metamagnetic transition from the antiferromagnetic state toward a field-induced ferromagnetially aligned phase at $B_C = 11.1\,\mathrm{T}$ is shifted to lower fields with increasing temperatures, in good agreement with previous results [14]. The transition exhibits a very narrow hysteresis around the transition field (~0.06 T at 1.5 K) in $\Delta f / f_{B=0}$. The hysteresis around B_c is believed to be real and it has been observed previously [19]. On the contrary, the differences in the values for $\Delta f / f_{B=0}$ above B_C are a function of dB/dt and the maximum applied field, and we tentatively attribute those to eddy-current heating during the field pulse. The metamagnetic transition disappears for temperatures above the Néel temperature, T_N = 19.3 K, but we still observed a change in the slope of $\Delta f / f_{B=0}$ even at temperatures well above T_N, e.g. a change in the slope of $\Delta f / f_{B=0}$ at T = 32.6 K at field about 25 T. This behavior is consistent with previously reported large magnetoresistance effects above T_N in UNiAl [19, 20]. In general, the magnetoresistance response in UNiAl and many other uranium compounds has been attributed to the suppression of AF fluctuations and to the disappearance of the magnetic superzones when the AF ordering is suppressed by magnetic field [14,21,22].

We took the anomalies in the measured relative frequency shift $\Delta f / f_{B=0}$ to extract the critical fields for the B-T magnetic phase diagram for B || c-axis in UNiAl. The results are shown as solid circles in Figure 3, which depicts the B-T phase diagram of UNiAl for fields applied along the *c* axis. Figure 3 also contains the metamagnetic transition fields, B_C, determined from the anomalies of our $\Delta f / f_{B=0}$ data, together with the results from previously reported specific heat [14], magnetization [14] and magnetoresistance [19] studies. For UNiAl, the boundary of the antiferromagnetic phase was established by specific-heat experiments in applied magnetic fields (solid line in Figure 3). However, magnetic and magnetoresistance results studies had revealed that short-range magnetic correlations persist well above T_N, and the inflection points of the magnetic isotherms occur well above the boundary when approaching T_N (dashed line in Figure 3). The B_C values determined from the anomalies in the measured relative frequency shift, $\Delta f / f_{B=0}$, are consistent with the B_C values determined from the inflection points of the magnetic isotherms and the results are in excellent agreement with the previously reported B-T phase diagram [14].

II. UNiGa

UNiGa is another UTX compound that crystallizes in the hexagonal ZrNiAl-type structure [1]. It shows a very complex magnetic phase diagram where multiple antiferromagnetic transitions are found between 35 and 40 K [23-29]. For all magnetic phases, the strong uniaxial anisotropy keeps the moments aligned along the *c*-axis. A relatively low magnetic field of less than 1 T applied along the *c*-axis induces metamagnetic transitions from the zero-field antiferromagnetic structures to uncompensated antiferromagnetic or a ferromagnetically-aligned phase.

Probably the most prominent and discussed feature in UNiGa is the large reduction of the electrical resistivity at the metamagnetic transition, especially for the current along *c*-axis where $\Delta\rho / \rho(0T) = 86\%$ [30]. Subsequently, we expect to observe a drastic change also in the frequency shift (Δf) at the metamagnetic transition in UNiGa.

Fig. 4 displays the anisotropic behavior of the measured relative frequency shift of the tank circuit $\Delta f / f_{B=0}$ for UNiGa as a function of applied magnetic fields at 4 K. Similar to UNiAl, application of a magnetic field has a little effect on $\Delta f / f_{B=0}$ for $B \perp c$-axis, while there is a strong dependence when the field is applied along the *c* axis. At 4 K, for fields applied along the *c* axis, we observed a slight change in the slope of $\Delta f / f_{B=0}$ at 0.25 T and a sudden reduction in the relative frequency shift (~1% of its zero-field value) at B_C = 0.88 T (see inset of Figure 4). The anisotropic behavior in $\Delta f / f_{B=0}$ for UNiGa is consistent with the magnetic anisotropy reported from previous single-crystal studies [23-29].

Fig. 5 shows the field dependence of the relative frequency shift of the tank circuit $\Delta f / f_{B=0}$ of UNiGa for fields applied along the *c*-axis at different temperatures. At 4 K, the change in the slope of $\Delta f / f_{B=0}$ at 0.25 T and the metamagnetic transition at B_C = 0.88 T move toward each other, join for temperatures around 20K, and then split again for higher temperatures.

Taking all the anomalies in measured relative frequency shift in the tank circuit, $\Delta f / f_{B=0}$, we extracted the critical field for $B \parallel c$-axis and included the results into the previously published B-T magnetic phase diagram for UNiGa. The result is shown in Figure 6, which is comprised out of our results (determined from the anomalies for $\Delta f / f_{B=0}$) and the results of previously published magnetic and neutron-diffraction results [25-29]. Clearly, our results are again in good agreement with previous data.

III. UNiGe

UNiGe crystallizes in the orthorhombic TiNiSi-type structure [1]. Unlike UTX compounds crystallizing in the hexagonal ZrNiAl structure, which exhibit strong uniaxial anisotropy, a variety of moment configurations are observed for different UTX compounds crystallizing in TiNiSi structure [1]. This indicates that the balance of exchange interactions is far more delicate in compounds with the TiNiSi structure than those with the ZrNiAl structure.

Bulk and neutron-diffraction studies on UNiGe indicated two antiferromagnetic transitions at about 42 and 50 K [31-38]. High-field magnetization measurements [34] showed that there are two metamagnetic transitions in UNiGe for field applied along *c*-axis (at 3 and 10 T) and two transitions with field along the *b*-axis (at 17 and 25 T). For the *a*-axis, the magnetization curve at 4.2 K is linear up to 38 T and the response is much weaker. Like in all other UTX compounds with TiNiSi structure, UNiGe shows a huge magnetic anisotropy. However, the magnetic anisotropy in this compound is interesting

because it is unusual to find that the *5f* moments have a significant component along the hard direction, which is contrary to expectations based on the models involving single-ion anisotropies of different sublattices [39].

Figure 7 displays the anisotropic behavior of the measured relative frequency shift in the tank circuit $\Delta f/f_{B=0}$ of UNiGe as a function of applied magnetic fields at 1.4 K. For fields applied along the *b* axis, there are three anomalies seen at 18 T, 24 T and 28 T in the field-up sweep. For fields applied along the *c* axis, two metamagnetic transitions were observed at 4.5 T and 9.5 T in the field-up sweep. Those results had been reported previously [40], but no comparison with B-T phase boundaries was done. For fields applied along the *a* axis, on the other hand, only a smooth and continuous decrease in $\Delta f/f_{B=0}$ is observed, which indicates that the *a* axis is the hard axis in UNiGe. The anisotropic response in $\Delta f/f_{B=0}$ for UNiGe is again consistent with the magnetic anisotropy inferred from previous single-crystal studies [34, 35].

Figure 8 shows the relative frequency shift of the tank circuit $\Delta f/f_{B=0}$ for UNiGe at various temperatures for fields applied along the *b* axis (Fig. 8a) and for fields applied along the c axis (Fig. 8b). For both orientations, only the lowest critical fields (at 1.4 K, B_c =18 T for B || *b*-axis and B_c = 4.5 T for B || *c*-axis) exhibits a strong suppression with increasing temperature, while the transitions at higher fields remain relatively flat up to ~35 K.

For B || *b*-axis, only two transitions around 17 and 25 T had been reported from previous magnetoresistance [34], while there was no report of a third transition. Since our sample was different than the one from ref. 34, we decided to check whether the occurrence of a third metamagnetic transition could be attributed to different samples or whether it might be an intrinsic property. To check this, we repeated the magnetoresistance measurement for B || *b*-axis on our sample, which was used for the RF skin-depth study. Figure 9 shows the measured magnetoresistance $\Delta\rho/\rho_{B=0}$ of UNiGe as a function of magnetic fields applied along the *b*-axis at different temperatures. At 5 K, $\Delta\rho/\rho_{B=0}$ exhibits only two metamagnetic transitions at 18.5 T and 26 T, in agreement with reports in ref. 34 on a different sample. Comparing $\Delta f/f_{B=0}$ and $\Delta\rho/\rho_{B=0}$ we can distinguish three metamagnetic transitions in the former measurement, while there are only two in the latter, although there is an additional weak change in the slope of $\Delta\rho/\rho_{B=0}$ at ~24 T. Moreover, we find an increase in $\Delta f/f_{B=0}$ at 24 T and 28 T but a decrease in $\Delta\rho/\rho_{B=0}$ at ~26 T. The different sign in the RF skin depth and the magnetoresistance response is unlike the behavior for B || c-axis in UNiGe, where sign the RF skin depth and the magnetoresistance are the same at both transition fields, as is the case also for UNiAl and UNiGa [10] i.e. the frequency shift mirrors the magnetoresistance. On the other hand, different behavior of $\Delta f/f_{B=0}$ and $\Delta\rho/\rho_{B=0}$ may not be too surprising because the frequency shift is sensitive to both the dielectric and magnetic properties, and it is conceivable that for particular field orientations the effects can be additive and while for other orientations the signs could be opposite.

Taking the anomalies for the relative frequency shift of the tank circuit $\Delta f/f_{B=0}$ and the magnetoresistance $\Delta\rho/\rho_{B=0}$ for UNiGe we extracted the transition field for B || *b*-axis and for B || *c*-axis. The extracted data were included in previously published B-T phase diagrams and the results are shown in Figure 10. The B-T phase diagrams contain our results and the previously published results from bulk magnetic and neutron diffraction studies [38]. Overall, the phase boundaries are in reasonable agreement with the previous reported phase boundaries [38, 41]. However, for B || b-axis, we observed a potential new phase (marked by '?'), which was not reported earlier. At this time, the nature of this phase is not clear.

Conclusion

In conclusion, we performed RF skin-depth measurements of antiferromagnetic UNiX compounds (X = Al, Ga, Ge) in magnetic fields up to 60 T applied along different crystallographic directions for temperatures between 1.4 and ~60 K. In most cases, there is a direct correspondence between the features in RF skin depth and magnetoresistance, and metamagnetic transitions are accompanied by drastic changes in both $\Delta f/f_{B=0}$ and $\Delta\rho/\rho_{B=0}$. This is indicative that both properties can be interpreted in terms of Fermi surface gapping due to the formation of magnetic superzones and/or due to spin-dependent scattering [10]. For all three compounds (UNiAl, UNiGa and UNiGe), the anomalies in $\Delta f/f_{B=0}$ corroborate the previously reported B-T phase diagrams for fields applied along different crystallographic directions.

Acknowledgements

The work was supported by a grant from NSF (Grant No: DMR-0804032). The NSF, the US Department of Energy and the State of Florida supported the work at the NHMFL, Los Alamos facility.

References

[1] V. Sechovsky, and L. Havela, in *Handbook of Magnetic Materials*, Vol. 11, edited by K.H.J. Buschow (Amsterdam) (1998).

[2] V. Sechovsky and L. Havela, in *Ferromagnetic Materials*, Vol. 4, eds E.P. Wohlfarth and K.H.J. Buschow, Amsterdam: North-Holland, 1988

[3] V. Sechovsky, L. Havela, P. Nozar, E. Brück, F.R. de Boer, A.A. Menovsky, K.H.J. Buschow and A.V. Andreev, Physica B, **163**, 103 (1990)

[4] K.H.J. Buschow, E. Brück, R.G. van Wierst, F.R. de Boor, L. Havela, V. Sechovsky, P. Nozar, E. Sugiura, M. Ono, M. Date and A. Yamagishi, J. Appl. Phys. **67**, 5216 (1990)

[5] R.A. Robinson, A.C. Larson, V. Sechovsky, L. Havela, Y. Kergadallan, H. Nakotte and F.R. de Boer, J. Alloys Comp. **213-314**, 528 (1994)

[6] N. W. Ashcroft and N. D Mermin, *Solid State Physics*, Saunders College Publishing, Fort Worth, 1976

[7] C. H. Mielke, J. Singleton, M. S. Nam, N. Harrison, C. C. Agosta, B. Fravel and L. K. Montgomery, J. Phys.: Cond. Mat. **13**, 8325 (2001)

[8] E. Ohmichi, E. Komatsu, and T. Osada, Rev. Sci. Instrum., **75** (6), 2094 (2004)

[9] C. H. Mielke, J. Singleton, M. S. Nam, N. Harrison, C. C. Agosta, B. Fravel and L. K. Montgomery, Nature (2008)

[10] A. M. Alsmadi, S. Alyones, C. H. Mielke, R. D. McDonald, V. Zapf, and M. M. Altarawneh, A. Lacerda, S. Chang, S. Adak, K. Kothapalli and H. Nakotte, J. Appl. Phys. (in press, 2009)

[11] C. T. van Degrift, Rev. Sci. Instrum., **46** (6), 599 (1975)

[12] L. Havela, V. Sechovsky, P. Nozar, E. Brück, F.R. de Boer, J.C.P. Klaasse, A.A. Menovsky, J.M. Fournier, M. Wulff, E. Sugiura, M. Ono, M. Date and A. Yamagishi, Physica B **136**, 313 (1990)

[13] K. Prokeš, F. Bourdarot, P. Burlet, P. Javorsky, M. Olsovec, V. Sechovsky, E. Brück, F.R. de Boer and A.A. Menovsky, Phys. Rev. B **58**, 2692 (1998)

[14] E. Brück, H. Nakotte, F.R. de Boer, P.F. de Chatel, H.P. van der Meulen, J.J.M. Franse, A.A. Menovsky, N.H. Kim-Ngan, L. Havela, V. Sechovsky, J.A.A.J. Perenboom, N.C. Tuan and J. Sebek, Phys. Rev. B **49**, 8852 (1994)

[15] V. Sechovsky, K. Prokeš, P. Svoboda, O. Syshchenko, O. Chernyavski, H. Sato, T. Fujita, T. Suzuki, M. Doerr, M. Rotter, M. Loewenhaupt and A. Gukasov, J. Appl. Phys. **89**, 7639 (2001)

[16] V. Sechovsky, L. Havela, L. Neuzil, A.V. Andreev, G. Hilscher and C. Schmitzer, J. Less-Common Met. **121**, 169 (1986)

[17] V. Sechovsky, L. Havela, F.R. de Boer, J.J.M. Franse, P.A. Veenhuizen, J. Sebek, J. Stehno and A.V. Andreev, Physica B **142**, 283 (1986)

[18] K. Prokeš, T. Fujita, N.V. Mushnikov, S. Hane, T. Tomita, T. Goto, V. Sechovsky, A.V. Andreev and A.A. Menovsky, Phys. Rev. B **59**, 8720 (1999)

[19] O. Mikulina, J. Kamarad, A. Lacerda, O. Syshchenko, T. Fujita, K. Prokeš, V. Sechovsky, H. Nakotte, W. Beyerman, A. A. Menovsky, J. Appl. Phys. **87**, 5152 (2000)

[20] F. Honda, V. Sechovsky, O. Mikulina, J. Kamarad, A.M. Alsmadi, H. Nakotte and A. Lacerda, Inter. J. Mod. Phys. B, **16**, 3330 (2002)

[21] F. Honda, K. Prokeš, G. Oomi, T. Kagayama, A.V. Andreev, V. Sechovsky, L. Havela, and E. Bruck, J. Phys. Soc. Jpn. **66**, 1904 (1997)

[22] K. Usami, J. Phys. Soc. Jpn. **45**, 466 (1978)

[23] V. Sechovsky, L. Havela, F. R. de Boer, E. Brück, T. Suzuki, S. Ikeda, S. Nishigori, and T. Fujita , Physica B **186-188**, 775 (1993)

[24] K. Prokeš, E. Brück, F. R. de Boer, M. Mihalik, A. Menovsky, P. Burlet, J. M. Mignot, L. Havela, V. Sechovsky, J. Appl. Phys. **79**, 6396 (1996)

[25] A. V. Andreev, L. Havela, V. Sechovsky, R. Kuzel, H. Nakotte, K.H.J. Buschow, J. H. V. J. Brabers, F.R. de Boer, E. Brück, M. Blomber, M. Merisalo, J. Alloys Comp. **224**, 244 (1995)

[26] L. Havela, V. Sechovsky, Y. Aoki, Y. Kobayashi, H. Sato, K. Prokeš, M. Mihalik, and A. A. Menovsky, J. Appl. Phys. **81**(8), 5778 (1997)

[27] Y. Kobayashi, Y. Aoki, H. Sugawara, H. Sato, V. Sechovsky, L. Havela, K. Prokeš, M. Mihalik, and A. A. Menovsky, Phys. Rev. B . **54**, 15330 (1996)

[28] F. Honda, K. Prokeš, M. Olšovec, F. Bourdarot, P. Burlet, T. Kagayama, G. Oomi, L. Havela, V. Sechovsky, A. V. Andreev, E. Brück, F.R. de Boer, A. A. Menovsky, and M. Mihalik, J. Alloys Comp. **224**, 244 (1995)

[29] V. Sechovsky, K. Prokeš, F. Honda, B. Ouladdiaf, and J. Kulda, Appl. Phys. A **74**, S834-S836 (2002)

[30] V. Sechovsky, L. Havela, K. Prokeš, H. Nakotte, F.R. de Boer, and E. Brück, J. Appl. Phys. **271-273**, 495 (1998)

[31] R. Troc and V.H. Tran, J.Magn. Magn. Mat. **73**, 389 (1988)

[32] A.P. Ramirez, B. Batlogg and E. Bucher, J. Appl. Phys. **61**, 3189 (1987)

[33] F. Canepa, P. Manfrinetti, M. Pani, A. Palenzona, J. Alloys Compounds **234**, 225 (1996)

[34] K. Prokeš, H. Nakotte, E. Brück, F.R. de Boer, L. Havela, V. Sechovsky, P. Svobada and H. Maletta, IEEE Trans. Magn. **30**, 1214 (1994)

[35] A. Purwanto, V. Sechovsky, L. Havela, R.A. Robinson, H. Nakotte, A.C. Larson, K. Prokeš, E. Brück and F. R. de Boer, Phys. Rev. B **53**, 758 (1996)

[36] V. Sechovsky, L. Havela, A. Purwanto, A.C. Larson, R.A. Robinson, K. Prokeš, H. Nakotte, E. Brück, F.R. de Boer, P. Svoboda, H. Maletta and M. Winkelmann, J. Alloys Comp. **293/294**, 536 (1994)

[37] H. Nakotte, A. Purwanto, R.A. Robinson, Z. Tun, K. Prokeš, A.C. Larson, L. Havela, V. Sechovsky and H. Maletta, Phys. Rev. B **54**, 7201 (1996)

[38] H. Nakotte, I.H. Hagmusa, J.C.P. Klaasse, M.S. Torikachvili, A.H. Lacerda, E. Brück, K. Prokeš, and F.R. de Boer, Physica B, **246-247**, 441 (1998)

[39] P.F. de Châtel, K. Prokeš, H. Nakotte, A. Purwanto, V. Sechovsky, L. Havela, E. Brück, R.A. Robinson and F.R. de Boer, J. Magn. Magn. Mater. **177-181**, 785 (1998)

[40] S. Chang, C. H. Mielke, M. Bennett, E. Brück, and H. Nakotte, Physica B, **312-313**, 877 (2002)

[41] F. R. de Boer, K. Prokeš H. Nakotte, E. Brück, M. Hilbers, P. Svoboda, V. Sechovsky, L. Havela, and H. Maletta, Physica B, **201**, 251 (1994)

Tables caption

Table 1. Crystal structures, ordering temperatures, T_N, and transition field(s), B_C, for UNiX compounds (X = Al, Ga and Ge) [1].

Compound	*Crystal structure*	T_N *(K)*	B_C *(T)*
UNiAl	Hexagonal ZrNiAl	19.3	11.1
UNiGa	Hexagonal ZrNiAl	34.1*	0.4-0.9
UNiGe	Orthorhombic TiNiSi	41.5	17 and 25 (*b*-axis) 3 and 10 (*c*-axis)

**three other transitions occur at slightly higher temperatures below 40 K*

Figures Captions

FIGURE 1

Field dependence of the relative frequency shift $\Delta f / f_{B=0}$ of the resonant tank circuit oscillations for UNiAl at 1.5 K with fields applied along (circles) and perpendicular to the c axis (triangles). For B|| c-axis, we observed a metamagnetic transition around $B_C = 11.1$ T, while no such transition is seen for fields up to 50 T for B $\perp$ c axis. Statistical errors are smaller than the symbols.

FIGURE 2

Field dependence of the relative frequency shift $\Delta f / f_{B=0}$ of the tank circuit oscillations for UNiAl with fields applied along the c axis at different temperatures. At 1.5 K, the frequency shift for both the up- and down-sweeps of the pulsed field is shown. For higher temperatures, only the results from up-sweeps are shown.

FIGURE 3

Magnetic B-T phase diagram of UNiAl for field applied along the c axis. Solid circles are taken from the anomalies of the relative frequency shift $\Delta f / f_{B=0}$ of the tank circuit, while crosses are the results from previously published data from specific heat and magnetoresistance studies [17]. The magnetic phases are labeled 'AF' for the antiferromagnetic phase, 'ferro' for the field-induced ferromagnetically-aligned phase and 'para' for the paramagnetic phase. Lines are guides to the eye. The boundary of the antiferromagnetic phase was established by specific-heat experiments in applied magnetic fields (solid line), but short-range magnetic correlations persist well above T_N (dashed line).

FIGURE 4

Field dependence of the relative frequency shift $\Delta f / f_{B=0}$ of the resonant tank circuit oscillations for UNiGa at 4 K with fields applied along (circles) and perpendicular to the c axis (triangles). For B || c-axis, we observed a slight change of slope around 0.25 T and a metamagnetic transition around $B_C = 0.85$ T, while no transition up to 50 T is found for B $\perp$ c axis. The inset shows the low-field response for B || c-axis.

FIGURE 5

Field dependence of the relative frequency shift $\Delta f / f_{B=0}$ of the tank circuit oscillations for UNiGa with fields applied along the c axis at different temperatures. Only field-up sweeps are shown.

FIGURE 6

Magnetic B-T phase diagram of UNiGa for field applied parallel to the c-axis. Solid circles are taken from the anomalies in the measured relative frequency shift $\Delta f / f_{B=0}$ in the tank circuit, and crosses represent previously published results from bulk magnetic and neutron-diffraction experiments [26]. The magnetic phases are labeled; '1' for incommensurate antiferromagnetic (AF) structure with a magnetic propagation vector $q \approx (0,0,0.36)$, '2' for an AF phase with $q = (0,0,1/3)$, '3' for an AF phase with $q = (0,0,1/8)$, 'AF-4' for the ground- state AF phase with $q = (0,0,1/6)$, '5' for the uncompensated antiferromagnetic phase with $q = (0,0,1/3)$, 'ferro-6' for the field-induced ferromagnetic phase with $q = (0,0,0)$, and 'para-7' for the paramagnetic phase. The shaded area represents a region where hysteresis effects occur. The lines are guides to the eye.

FIGURE 7

Field dependence of the relative frequency shift $\Delta f / f_{B=0}$ of the resonant tank circuit oscillations for UNiGe at 1.4 K with magnetic fields applied along a, b and c-axes, represented by diamonds, triangles and circles, respectively.

FIGURE 8

Field dependence of the relative frequency shift $\Delta f / f_{B=0}$ of the tank circuit oscillations for UNiGe at various temperatures with magnetic fields applied along a) the b axis and b) the c axis.

FIGURE 9

Field dependence of the relative magnetoresistance $\Delta\rho / \rho_{B=0}$ for UNiGe for fields applied along the b axis at different temperatures.

FIGURE 10

Magnetic phase diagram of UNiGe for fields applied a) along the b axis and b) along the c axis. Solid circles are taken from the anomalies of the relative frequency shift $\Delta f / f_{B=0}$ of the tank circuit, solid squares are taken from the anomalies of the here

measured relative magnetoresistance $\Delta\rho/\rho(B=0)$, and crosses represent the previously published magnetoresistance data [38]. The magnetic phases are labeled incommensurate 'IC' with $q \approx (0,\delta,\delta)$, the field-induced uncompensated antiferromagnet 'UAF' with $q = (0,1/3,1/3)$, the antiferromagnetic ground state 'AF' with $q = (0,1/2,1/2)$ phase, the field-induced ferromagnetically-aligned phase 'ferro', the paramagnetic phase 'para' and the unknown phase '?'. The shaded area in b) represents a region where hysteresis effects occur. Lines are guides to the eye.

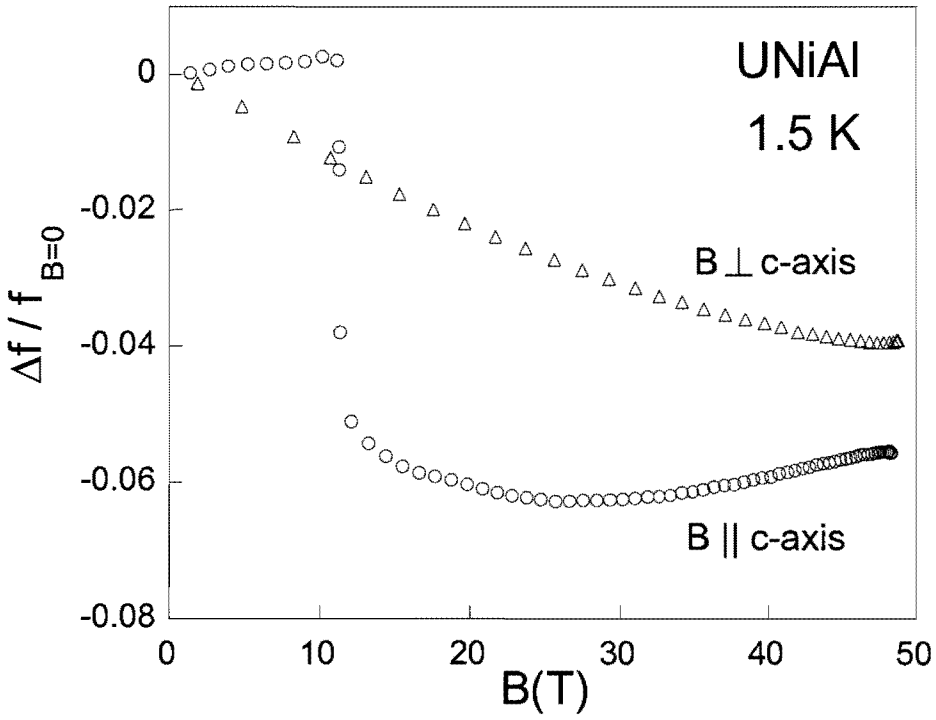
UNiAl
1.5 K
B ⊥ c-axis
B || c-axis
0
-0.02
-0.04
-0.06
-0.08
Δf / f B=0
0
10
20
30
40
50
B(T)

Fig. 1.

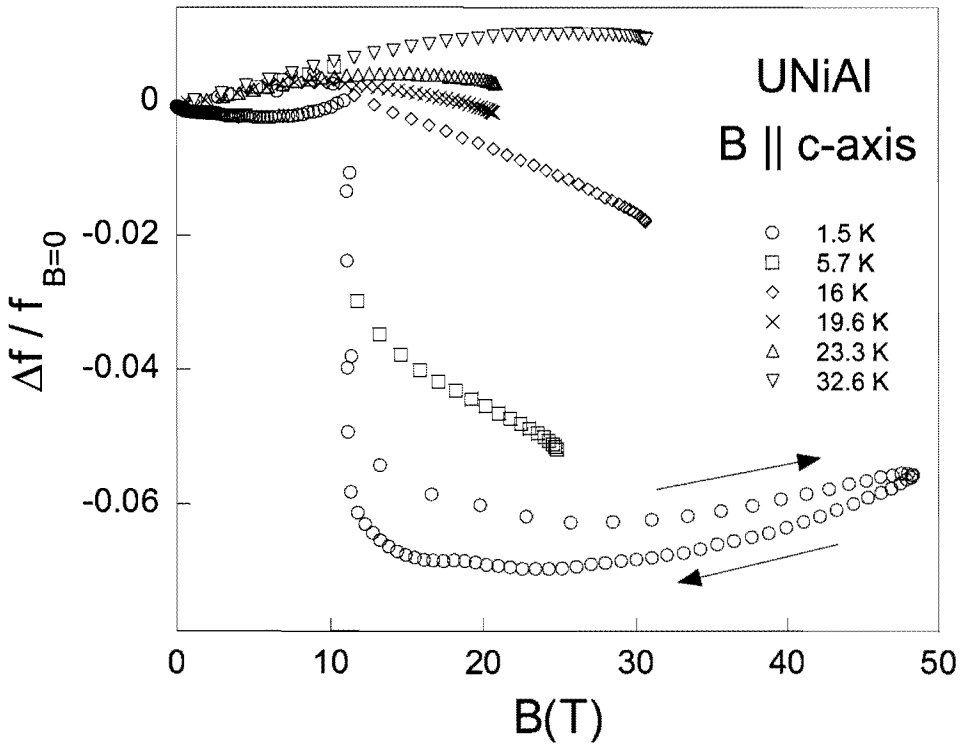
UNiAl
B || c-axis
1.5 K
5.7 K
16 K
19.6 K
23.3 K
32.6 K
0
-0.02
-0.04
-0.06
Δf / f B=0
0
10
20
30
40
50
B(T)

Fig.2.

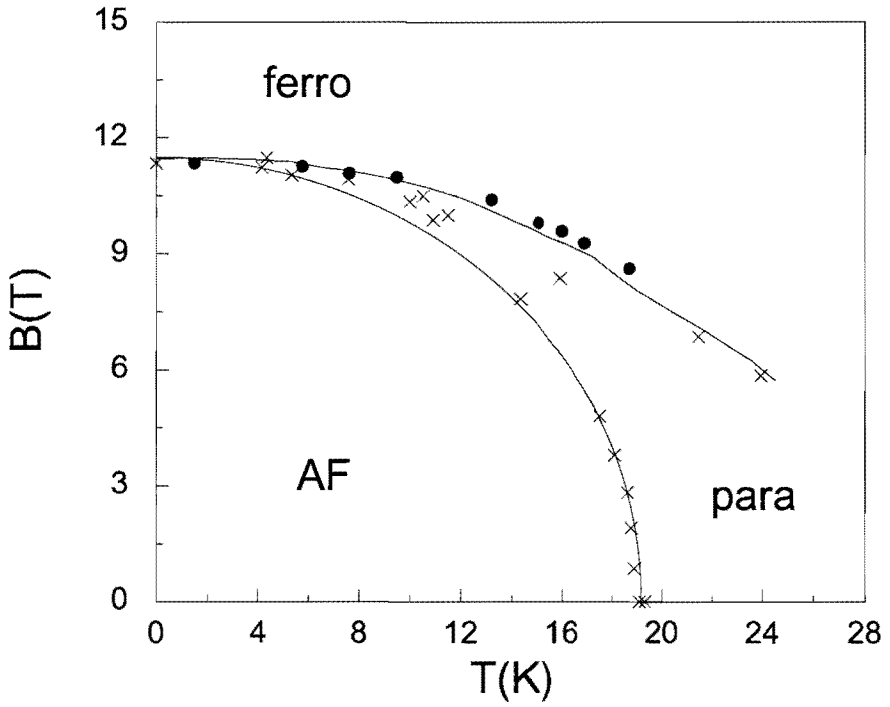
ferro
AF
para
B(T)
T(K)
15
12
9
6
3
0
0
4
8
12
16
20
24
28

Fig.3.

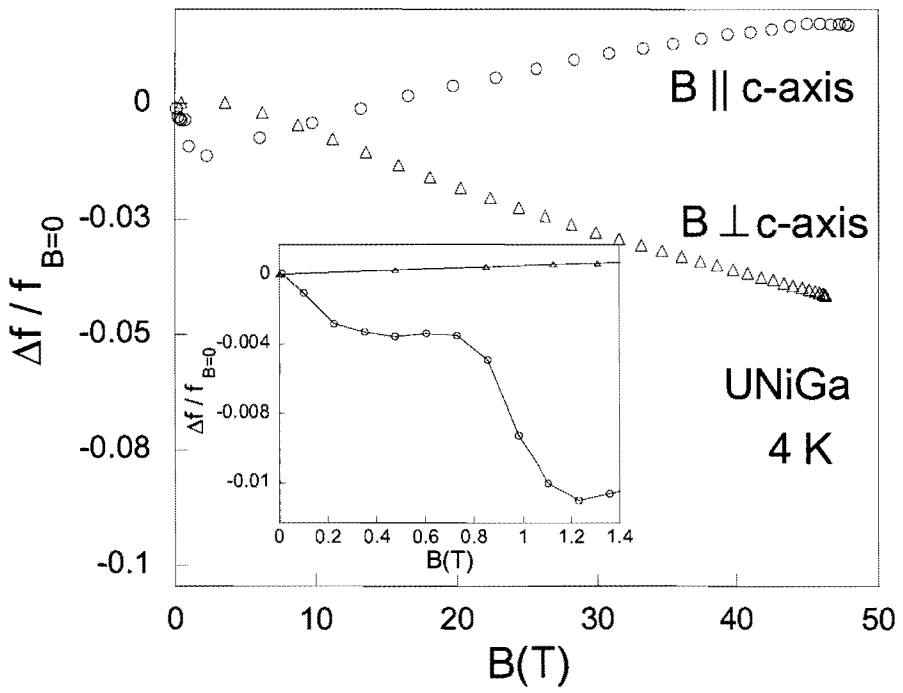
B || c-axis
B ⊥ c-axis
UNiGa
4 K
Δf / f B=0
B(T)
0
-0.03
-0.05
-0.08
-0.1
0
10
20
30
40
50
-0.004
-0.008
-0.01
0.2
0.4
0.6
0.8
1
1.2
1.4

Fig.4.

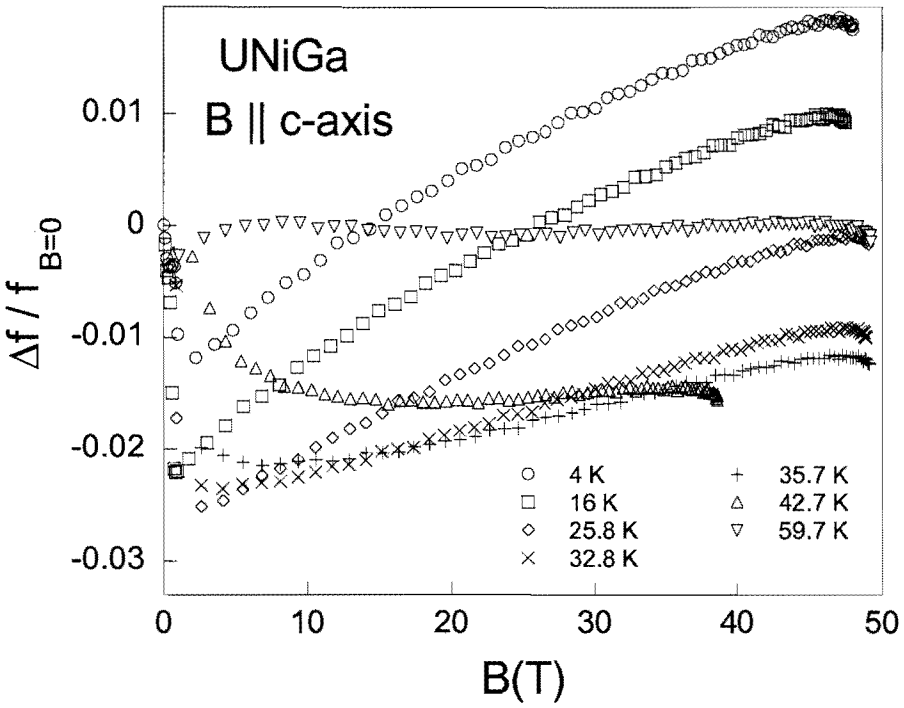
UNiGa
B || c-axis
0.01
0
-0.01
-0.02
-0.03
Δf / f B=0
0
10
20
30
40
50
B(T)
4 K
16 K
25.8 K
32.8 K
35.7 K
42.7 K
59.7 K

Fig.5.

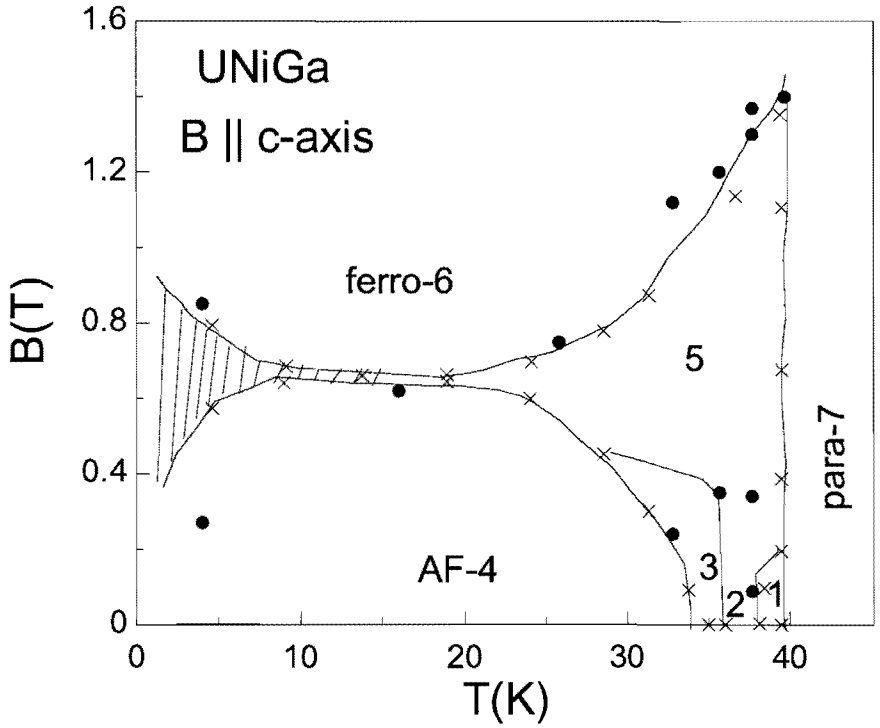
UNiGa
B || c-axis
1.6
1.2
0.8
0.4
0
B(T)
0
10
20
30
40
T(K)
ferro-6
5
AF-4
3
2
1
para-7

Fig. 6.

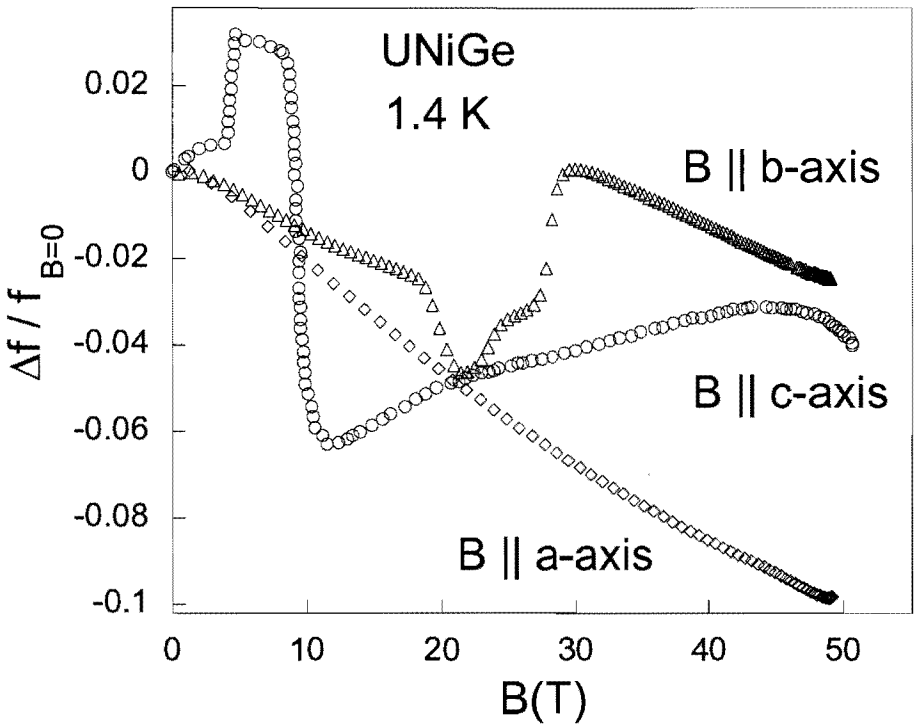
UNiGe
1.4 K
B || b-axis
B || c-axis
B || a-axis
0.02
0
-0.02
-0.04
-0.06
-0.08
-0.1
Δf / f B=0
0
10
20
30
40
50
B(T)

Fig. 7.

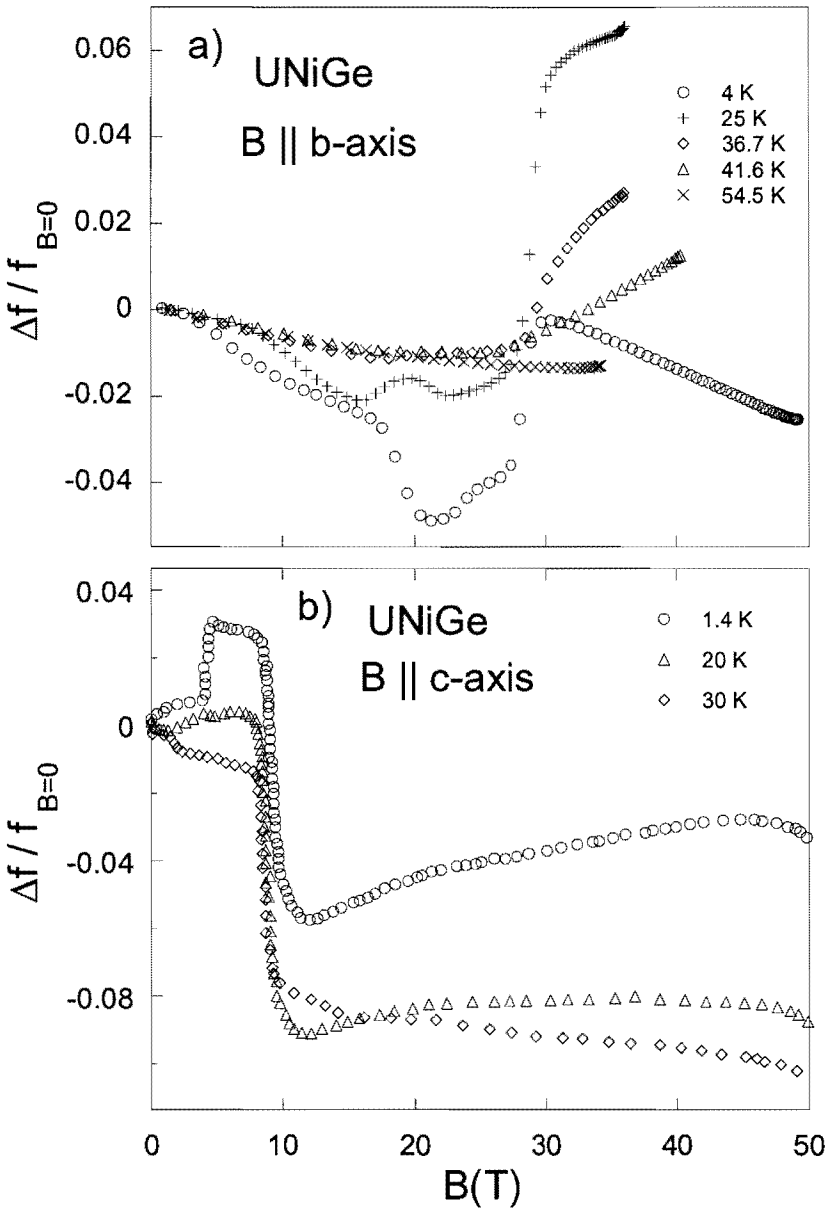
a)
UNiGe
B || b-axis
4 K
25 K
36.7 K
41.6 K
54.5 K
0.06
0.04
0.02
0
-0.02
-0.04
Δf / f B=0
b)
UNiGe
B || c-axis
1.4 K
20 K
30 K
0.04
0
-0.04
-0.08
Δf / f B=0
0
10
20
30
40
50
B(T)

FIG. 8.

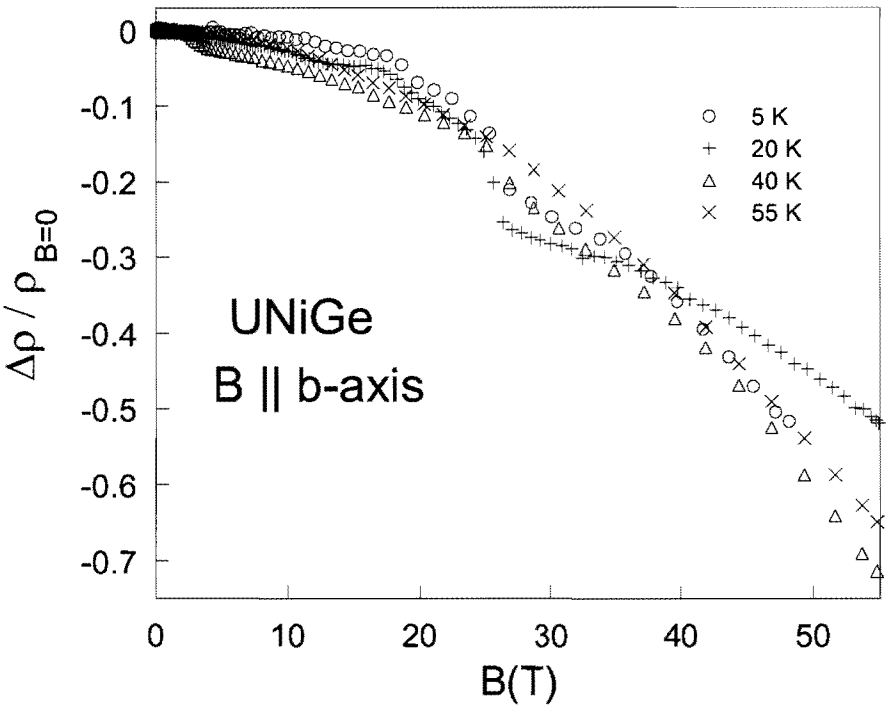
0
-0.1
-0.2
-0.3
-0.4
-0.5
-0.6
-0.7
Δρ / ρ B=0
UNiGe
B || b-axis
5 K
20 K
40 K
55 K
0
10
20
30
40
50
B(T)

FIG. 9.

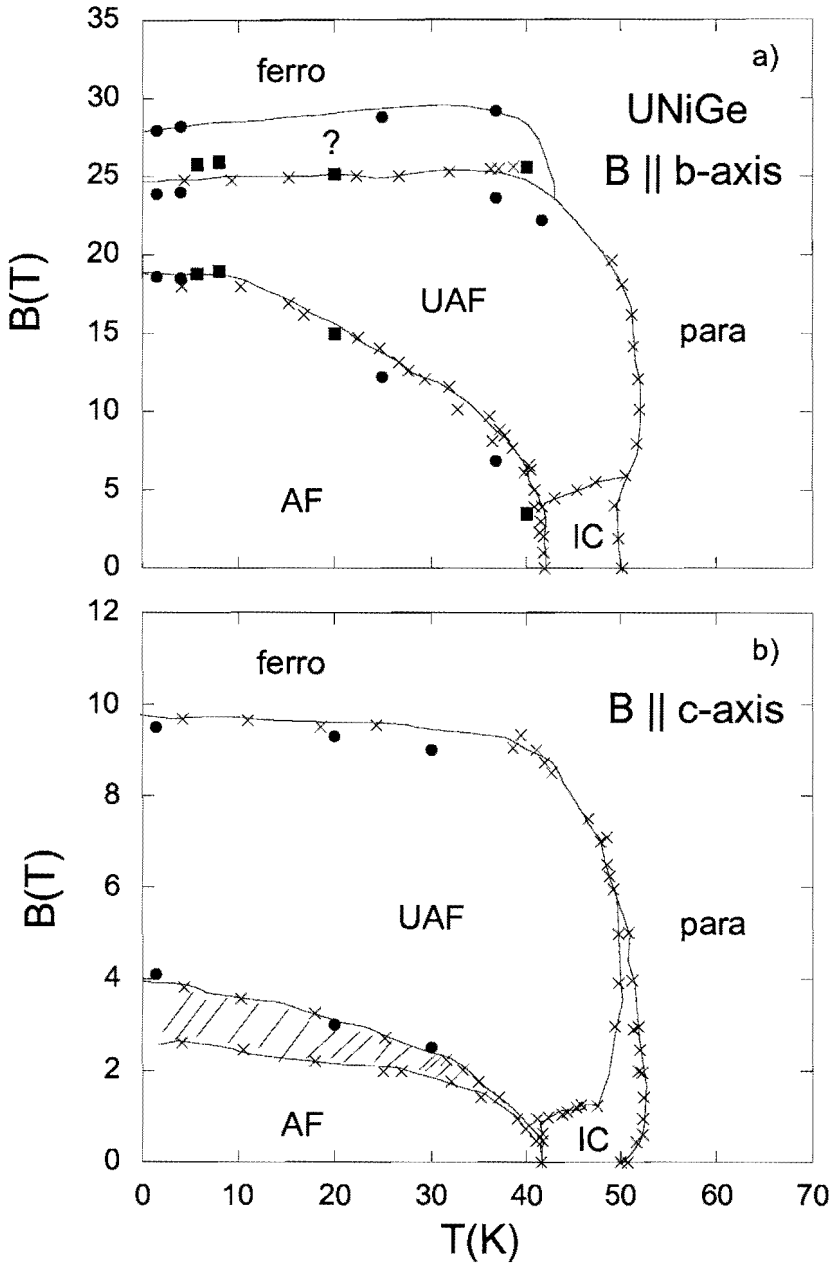
a)
ferro
?
UNiGe
B || b-axis
UAF
para
AF
IC
B(T)
b)
ferro
B || c-axis
UAF
para
AF
IC
B(T)
T(K)

FIG.10.